

Communication

# An Optical Spectroscopic Study of Air-Degradation of van der Waals Magnetic Semiconductor Cr<sub>2</sub>Ge<sub>2</sub>Te<sub>6</sub>

Woye Pei <sup>1,†</sup>, Zhiren Xiong <sup>1,2,†</sup>, Yingjia Liu <sup>3,4,†</sup>, Xingguang Wu <sup>1,2</sup>, Zheng Vitto Han <sup>1,2,5</sup> , Siwen Zhao <sup>3,4,5,\*</sup> and Tongyao Zhang <sup>1,2,\*</sup>

<sup>1</sup> State Key Laboratory of Quantum Optics and Quantum Optics Devices, Institute of Opto-Electronics, Shanxi University, Taiyuan 030006, China

<sup>2</sup> Collaborative Innovation Center of Extreme Optics, Shanxi University, Taiyuan 030006, China

<sup>3</sup> Shenyang National Laboratory for Materials Science, Institute of Metal Research, Chinese Academy of Sciences, Shenyang 110016, China

<sup>4</sup> School of Material Science and Engineering, University of Science and Technology of China, Hefei 230026, China

<sup>5</sup> Liaoning Academy of Materials, Shenyang 110016, China

\* Correspondence: swzhao@imr.ac.cn (S.Z.); tongyao\_zhang@sxu.edu.cn (T.Z.)

† These authors contributed equally to this work.

**Abstract:** Two-dimensional (2D) magnetic semiconductors exhibit unique combination of electronic and magnetic properties, holding great promise in potential applications such as spintronics and magneto-optics. However, many of them are air-sensitive, and their properties can be significantly altered upon exposure to air. Here, we showed an optical spectroscopic investigation of the effects of air-degradation on few-layered van der Waals (vdW) magnetic semiconductor Cr<sub>2</sub>Ge<sub>2</sub>Te<sub>6</sub>. It was found that although the partially degraded few-layered Cr<sub>2</sub>Ge<sub>2</sub>Te<sub>6</sub> showed a significant Raman red-shift and a split of E<sub>g</sub> peak at room temperature, the magneto-optic Kerr hysteresis loop can remain largely unchanged below the Curie temperature. Temperature-dependent Raman measurements further revealed characteristic blueshifts of phonon energy, which were associated with the ferromagnetic phase transition in partially degraded Cr<sub>2</sub>Ge<sub>2</sub>Te<sub>6</sub>, in agreement with Kerr measurements. Our results provide an optical spectroscopic insight into the air-instability of 2D magnetic semiconductors, and contribute to a better understanding of the relationship between phonon modes and long-range spin order at the presence of defects in ultra-thin vdW magnetic semiconductors.

**Keywords:** air stability; Cr<sub>2</sub>Ge<sub>2</sub>Te<sub>6</sub>; Raman spectrum; 2D magnetic semiconductor



**Citation:** Pei, W.; Xiong, Z.; Liu, Y.; Wu, X.; Han, Z.V.; Zhao, S.; Zhang, T. An Optical Spectroscopic Study of Air-Degradation of van der Waals Magnetic Semiconductor Cr<sub>2</sub>Ge<sub>2</sub>Te<sub>6</sub>. *Magnetochemistry* **2023**, *9*, 104. <https://doi.org/10.3390/magnetochemistry9040104>

Academic Editor: Roberto Zivieri

Received: 6 March 2023

Revised: 27 March 2023

Accepted: 4 April 2023

Published: 10 April 2023



**Copyright:** © 2023 by the authors. Licensee MDPI, Basel, Switzerland. This article is an open access article distributed under the terms and conditions of the Creative Commons Attribution (CC BY) license (<https://creativecommons.org/licenses/by/4.0/>).

## 1. Introduction

Layered vdW semiconducting materials with long-range spin orders attracted widespread attentions due to their unique physical properties [1–4]. The easy exfoliation nature of these 2D semiconducting flakes with intrinsic magnetism make it not only a candidate for spin-based devices (such as spin field effect transistors [5], spintronic memory [6], and all-spin logic devices [7]), but also vertically stackable with other vdW layers to construct nano-architectures for novel interlayer coupling of 2D materials [8]. Among them, few-layered Cr<sub>2</sub>Ge<sub>2</sub>Te<sub>6</sub> (CGT) is of special interest due to its perpendicular magnetic anisotropy and gate-tunable semiconducting electrical properties below its Curie temperature, which led to several conceptual nanoelectronic and optoelectronic devices [9].

It is known that the air-stability of 2D vdW layered magnetic materials is crucial for realizing the stable performance of nanodevices based on them [10]. Regrettably, the stability of most of magnetic materials with a thickness of one or a few atoms is barely satisfactory, as they are easily affected by the external environment and reduce their performance (such as temperature, stress, etc.) [11–14] as a consequence. Belonging to Telluride, CGT is easily degraded in air by reaction with oxygen to form TeO<sub>x</sub>, which

accelerates as the temperature increases [10–19]. For 2D CGT, its monolayer (1L) rapidly degrades and becomes invisible under the optical microscope, while the exfoliation of bilayer CGT flakes was feasible and was found to be robust over 90 min in ambient atmosphere, with no traceable degradation [20]. To protect few-layered CGT samples, the preparation process are often carried out in a glove box filled with inert atmosphere and the encapsulating layers (such as h-BN, MgO, Al<sub>2</sub>O<sub>3</sub>, and other noble metals) [21,22] will be needed to minimize the contact time with O<sub>2</sub> and H<sub>2</sub>O [23]. Despite meticulous sample fabrication, 2D CGT inevitably degrades, leading to significant alterations in its physical properties. This can result in inaccurate interpretations of experimental results, highlighting the need for comprehensive studies on degradation-related CGT to address this issue.

In this work, we prepared vdW heterostructures of few-layered CGT in pristine and partially degraded conditions, respectively, with encapsulated by hexagonal boron nitride (h-BN). We measured the hysteresis loops of the two samples separately, which indicated that air degradation has marginal effects on the magnetic properties of the CGT samples. Nevertheless, the Raman spectra, characterized as a function of temperature, demonstrated a pronounced effect of air degradation on the phonon modes of CGT lattices.

## 2. Materials and Experiments

To construct h-BN/CGT/h-BN heterostructures, high-quality CGT single crystals were used with XRD and EDS verification, as plotted in Figures 1a and 1b, respectively. h-BN flakes were mechanically exfoliated from bulk crystal onto SiO<sub>2</sub>/Si<sup>++</sup> substrates, with thicknesses of 20–30 nm selected by using atomic force microscopy (Figure 1e,f). Few-layered CGT flakes were exfoliated onto PDMS in a glove box with O<sub>2</sub> and H<sub>2</sub>O levels below 0.1 ppm and their thicknesses were identified by optical contrasts. The pristine CGT samples of 5–10 nm were transferred onto selected h-BN flakes with another h-BN further picked up and transferred onto the CGT/h-BN heterostructure by using PPC (Propylene-Carbonate) to form h-BN/CGT/h-BN sandwich structure (Figure 1d) [23]. The thickness of 5–10 nm was chosen because the Raman intensity of CGT nanosheets increased significantly with decreasing thickness due to the onset of interference effects. However, CGT that is too thin is more likely to oxidize and lead to the disappearance of Raman modes [24–27]. For CGT samples with partial degradation, CGT on PDMS were intentionally placed in ambient environment for several hours and transited to the glove box to complete the residual fabrication as mentioned above. In order to eliminate the influence of other factors, the tested samples all adopted the same h-BN-encapsulation CGT structure as shown in Figure 1c [28].

To explore the effect of air degradation on few-layered CGT, we mainly focused on the magnetic and optical properties of the samples which were mounted in a helium-free optical cryostat with accurate *x-y-z* piezo positioner and high numerical aperture objective. For room temperature measurements, we pumped the optical cryostat to a vacuum below 0.7 torr before measuring the Raman spectrum. An input laser ( $\lambda = 532$  nm) with controllable power ( $\sim 1$  mW) was focused on the samples with a spot size of about 2  $\mu\text{m}$ , and the scattered signal passing through a long wave pass filter was collected by a spectrometer equipped with a liquid-nitrogen cooled CCD (Horiba iHR550). In order to clean up the spectrum of excitation laser, we added a bandpass filter on the optical path of incident light to minimize the stray light on the detection of Raman signals. In order to perform polarization-resolved Raman measurements of the partially degraded CGT, we inserted a polarizer and a half-wave retardance in the incident optical path to control the polarization of excitation laser. The scattered light was analyzed by another polarizer in the reflected optical path. This way, we only needed to rotate the half-wave retardance to control the polarization angle of the excitation laser with respect to the detection of scattered light. The polarization of the polarizer and analyzer were both kept horizontal. Therefore, we rotated the half-wave retardance to adjust polarization angle and measured Raman spectrum every 10 degrees within the 360 degrees range of the laser polarization.

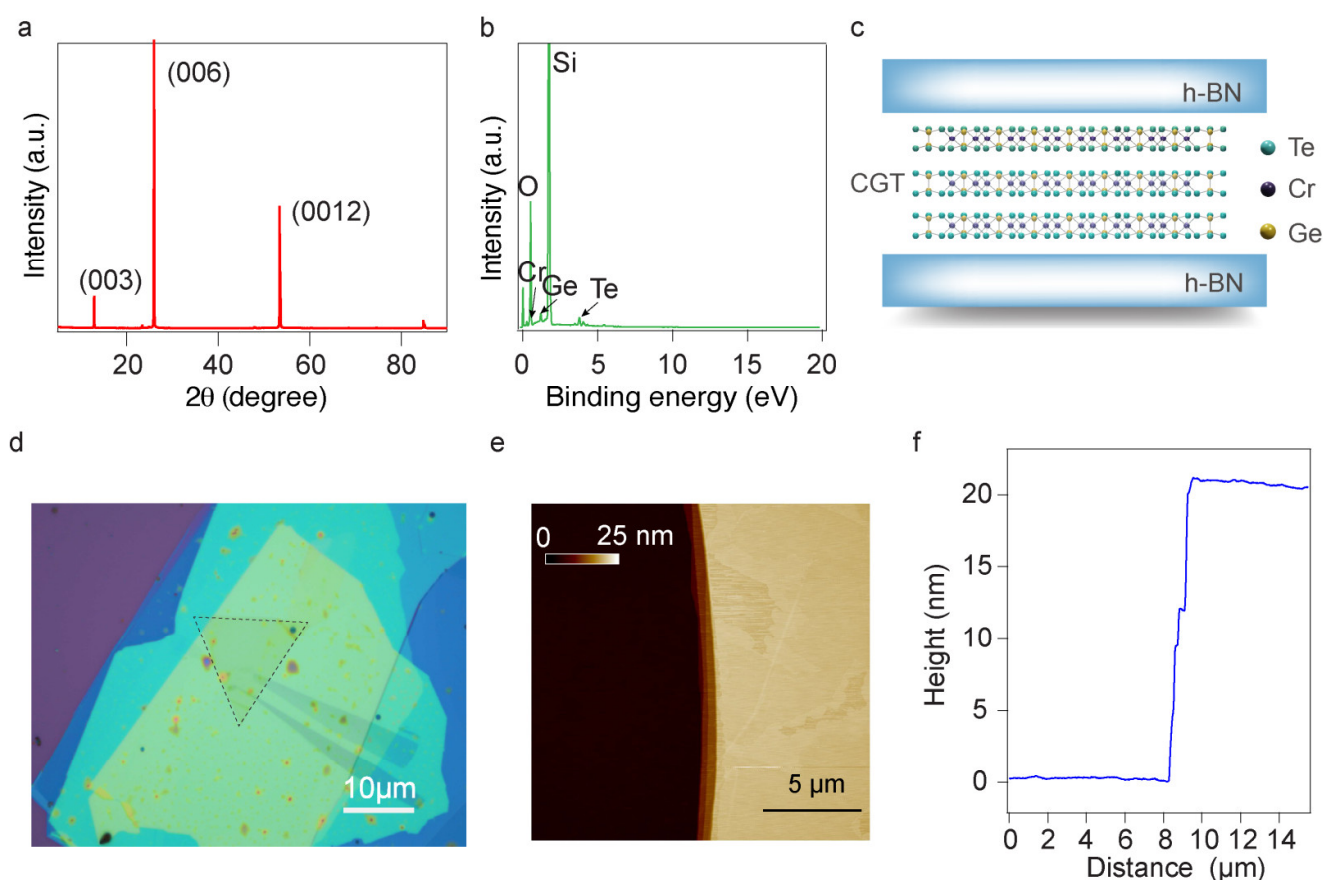


**Figure 1.** The results of XRD (a) and EDS (b) measurement, respectively, confirming the crystal structures and element ratios of bulk CGT. (c) Schematic diagram of h-BN encapsulated CGT heterostructure. (d) The optical photograph of a partially degraded CGT sample. CGT flake is sandwiched by top and bottom h-BN, with the edge of the CGT crystal indicated by the black dashed lines. Scale bar is 10 μm. (e) AFM profiles of a typical h-BN used to compose the sandwiched CGT heterostructure. (f) The linecut of the morphology in (e) to determine the thickness of the h-BN.

We studied the temperature dependence of Raman spectra on two kinds of samples separately by cooling down the optical cryostat. The pristine CGT was measured every 10 K in the range of 10–140 K, and the Raman spectrum of partially degraded CGT was measured in the same temperature range with much smaller intervals. Since temperature changes and other influencing factors will cause slight drift of the sample position in the optical cryostat, we adjusted the sample position and coupled the spectrometer every time after temperature changed to ensure the consistency of the measurement position.

The magneto-optic Kerr experiments were performed in the same closed-cycle optical cryostat equipped with the same objective and laser as Raman measurements. The probe laser of 2 μW was kept in linear polarization and focused on the sample surface in Faraday geometry with an out-of-plane magnetic field applied. A polarization sensitive system composed by a half-wave retardance and a Wollaston prism analyzed the reflected laser which was detected by a balanced photoreceiver.

### 3. Results and Discussion

Typical Raman spectra are shown in Figure 2a. The pristine CGT exhibited two characteristic peaks located at  $110.1\text{ cm}^{-1}$  and  $135.9\text{ cm}^{-1}$ , which were named as  $E_g^2$  and  $A_g^1$ , respectively [29]. CGT is a rare example of layered chalcogenides with the R-3 (No. 148) space group and the  $C_{3i}$  point group. Here, both two modes were Raman active the  $E_g^2$  mode was doubly degenerate and the  $A_g^1$  mode was nondegenerate, the  $E_g^2$  mode involved the twisting vibration of Cr–Ge octahedra and the shear vibration of the Ge atoms, while

the  $A_g^1$  mode involved the rocking vibration of three Te atoms around one Cr atom and the stretching vibration of two Ge atoms [30–33]. In contrast to the scenario of pristine samples, three Raman peaks (indicated by solid black triangles) were seen in partially degraded CGT, as shown in Figure 2a. It should be noted that after analysis and Gaussian fitting, it was found that the second Raman peak was composed of two vibration modes. We thus named them  $P_1$ ,  $P_2$ ,  $P_3$ ,  $P_4$ , respectively. We also tested the polarization dependence of the four peaks  $P_1$ – $P_4$ . Polar plots of the intensity Raman modes with respect to polarization angles are shown in Figure 2b–e. The peak changes of these four vibration modes were all in the shape of a dumbbell, revealing a nondegenerate nature of these modes.

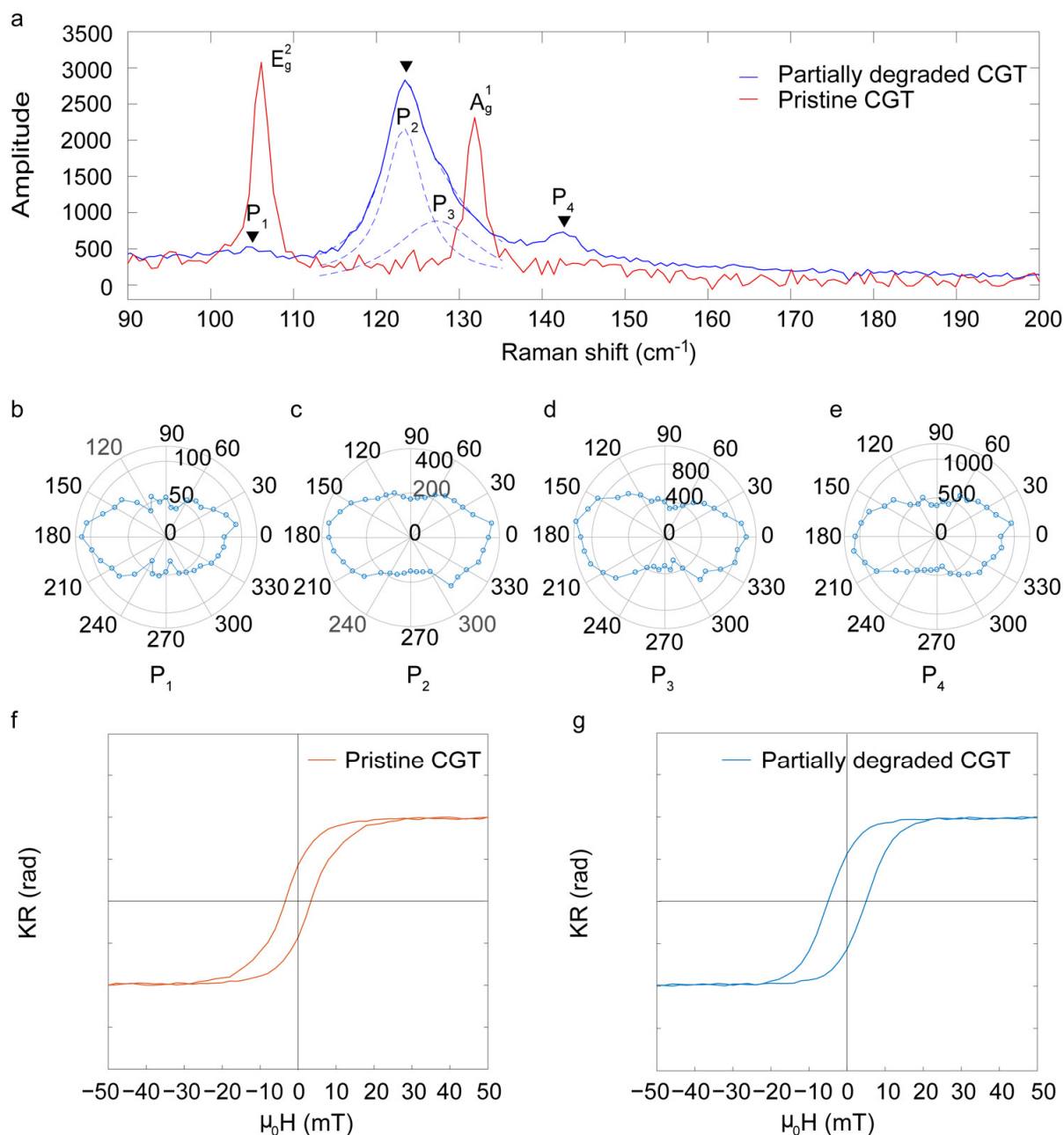


**Figure 2.** (a) Raman spectrum of pristine CGT and partially air-degraded CGT taken at  $T = 294$  K. (b–e) are the polarization angle-dependent Raman intensity of the  $P_1$ ,  $P_2$ ,  $P_3$ , and  $P_4$  modes, respectively. (f) Magnetic hysteresis loop of pristine CGT at 10 K. (g) Magnetic hysteresis loop of partially degraded CGT at 10 K.

We now come to the effects of air-degradation on magnetism in few-layered CGT. The magnetic hysteresis loops of two samples were tested at 10 K, as shown in Figure 2f,g, which was in agreement with the literature [34,35]. It was seen that the magnetic hysteresis loop of partially degraded CGT samples were almost unchanged as compared to those of pristine ones. It was thus concluded that the ferromagnetic spin ordering of the CGT sample had a certain stability against defects, and the air degradation to some extent will have only a limited impact on the magneto-optic Kerr signals.

We further studied the differences between pristine samples and partially degraded samples, as a function of temperature. The temperature dependence of long-range ferromagnetic order of CGT was widely investigated previously [20]. Here, we first tested the Raman spectra of the two samples at various temperatures in the range of 10–140 K, shown in Figures 3a and 3b, respectively. At the temperature of about 60 K, an abrupt change of peak position (indicated by black solid arrow in Figure 3c) in the Raman spectrum for both pristine CGT and partially degraded CGT was observed. This was mainly because of the Curie temperature  $T_C$  of CGT, which underwent a phase transition from random to ordered spin texture and further changes the phonon modes, resulting in a large shift of the peak before and after  $T_C$ . The temperature dependent phonon mode positions above  $T_C$  can be modeled by the following equation [20]:

$$v(T) = v(0) + A \left[ 1 + \frac{2}{(e^{hv(0)/2k_B T} - 1)} \right] \quad (1)$$

where  $v(0)$  is the extrapolation of optical phonon energy at 0 K. We fitted the peak position of P<sub>2</sub> above ~70 K well by using Equation (1), shown as the dashed line in Figure 3c.

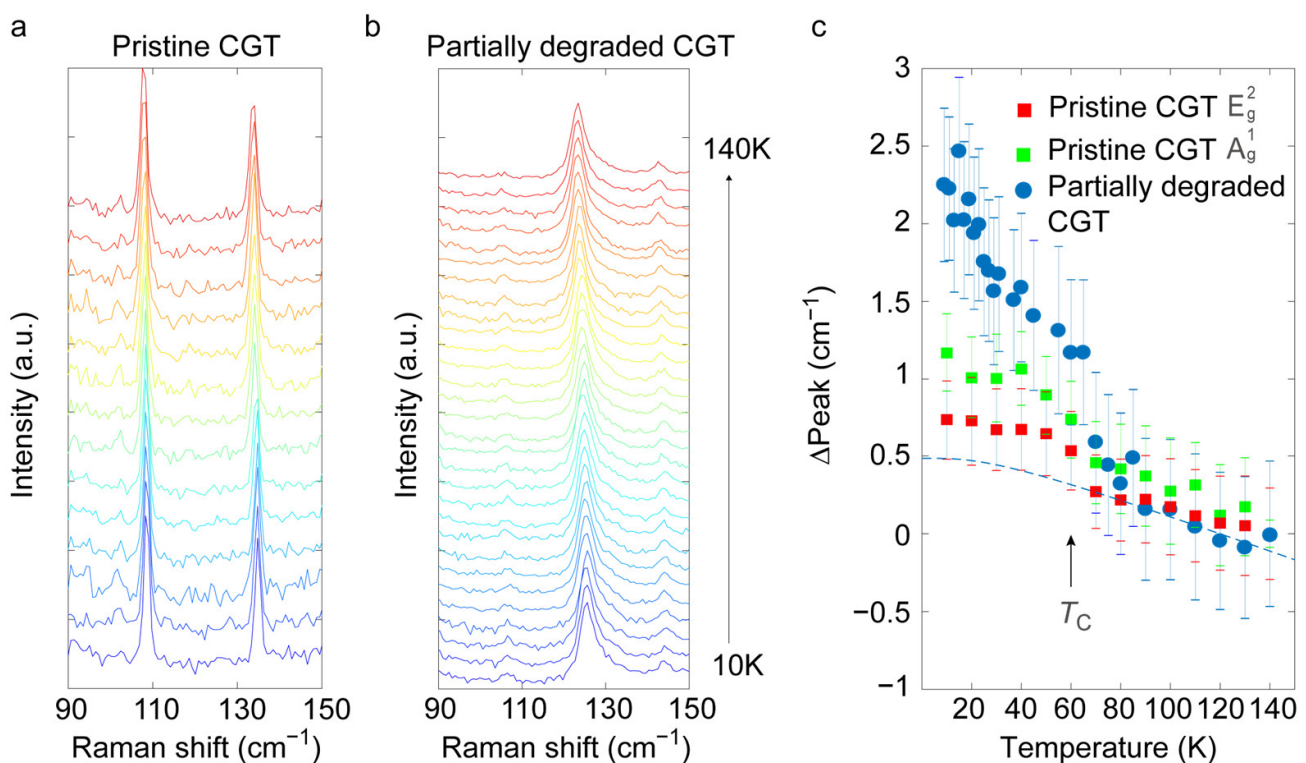


**Figure 3.** (a) Raman spectrum of pristine sample 10 K–140 K. (b) Raman spectrum of partially degraded sample 10 K–140 K. (c) The peak position of two modes  $E_g^2$  and  $A_g^1$  for pristine CGT, and P<sub>2</sub> for partially degraded CGT, traced from 10 K to 140 K. Error bars denote the uncertainty of the fittings. Dashed line is a fit according to Equation (1).

Notice that the observed  $T_C$  in our experiment is in good agreement with previously reported [15,33,34]. It suggests that even though the Raman peak position dramatically changed in the partially degraded CGT samples, it still exhibited the feature related to magnetic phase transition. Therefore, it is of importance to note that in characterizations of 2D magnetic materials, a signature of ferromagnetism does not necessarily mean the material is in a pristine state.

We now discuss the widths of the  $P_2$ – $P_4$  peaks of partially degraded CGT and the  $E_g^2$  and  $A_g^1$  peaks of pristine CGT at different temperatures, as shown in Figure 3a,b. The Raman peak widths of the pristine CGT were in general narrower compared to degraded sample, and there was negligible change with the variation of temperature, and the peak width of the  $E_g^2$  and  $A_g^1$  were comparable, which is in good agreement with the results reported previously [29]. However, the peak widths of the partially degraded CGT peaks were significantly different from its pristine state.  $P_2$  in partially degraded CGT showed a peak width comparable to that of  $E_g^2$  and  $A_g^1$  in the pristine CGT, with little dependence on temperature. Nevertheless,  $P_3$  and  $P_4$  of partially degraded CGT had significantly larger widths, which may be related to the formation of oxides on the surface [18,36].

Except for the temperature-dependent Raman, we also carried out temperature-dependent magneto-optic Kerr measurement in partially degraded CGT samples (while the Kerr data of pristine CGT can be found in studies such as Ref. [8] and Refs. [22,23]). As plotted in Figure 4a, the magneto-optic Kerr loops recorded in the temperature range of 5 to 45 K showed ferromagnetic characteristics at the base temperature, which gradually became paramagnetic with increasing the temperature. Figure 4b shows saturated magnetization ( $M_S$ , defined as 95% of the maximum Kerr angle around 50 mT) of each curve in Figure 4a. It was seen that the sample exhibited non-detectable  $M_S$  above 40 K, which was lower than the  $T_C$  (~60 K) of partially degraded CGT obtained by Raman measurements. We must emphasize that due to instrumental noise limit, the magnetic phase transition temperature might have been underestimated using magneto-optic Kerr. However, the key observation here is that even in degraded CGT sample (which has totally different Raman signals compared to the pristine state), magnetic characteristics (i.e., magnetic hysteresis loops, as well as the Curie temperature) were still robust and detectable by various optical spectroscopic detections.

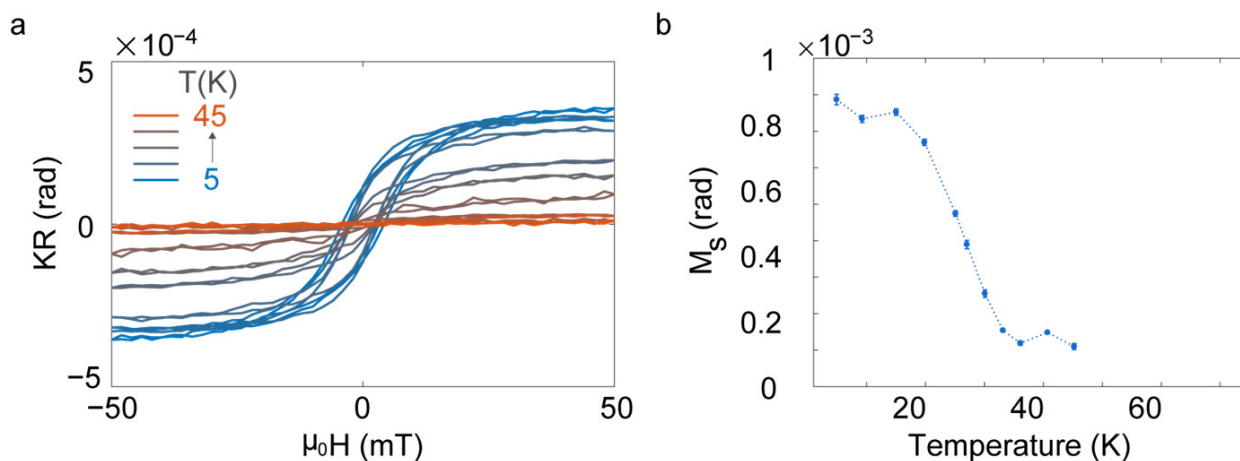


**Figure 4.** (a) Magneto-optic Kerr hysteresis loops at different temperatures, measured in a partially degraded CGT sample. (b) Saturated magnetization of CGT versus temperature. Error bars denote the standard deviation of saturated magnetization.

#### 4. Conclusions

In conclusion, our study provided a detailed optical spectroscopic investigation into the air-degradation effects on few-layered van der Waals magnetic semiconductor  $\text{Cr}_2\text{Ge}_2\text{Te}_6$ . The observed significant alterations in Raman spectra upon exposure to air highlighted the air-instability of 2D magnetic semiconductors. However, the temperature-dependent Raman measurements revealed that a shift of peak position associated with the ferromagnetic phase transition  $\text{Cr}_2\text{Ge}_2\text{Te}_6$  can still be found in degraded CGT samples, just like the pristine ones. The characteristic of ferromagnetism in degraded CGT samples was then further confirmed by the magneto-optic Kerr measurements, as the hysteresis loop remained largely unchanged below the Curie temperature in degraded CGT, with a rather well-defined  $T_C$ . Our results underscore the importance of considering the air-sensitivity and potential degradation of 2D magnetic materials in their characterizations, as the presence of ferromagnetism does not necessarily indicate a pristine state.

**Author Contributions:** Conceptualization, methodology, formal analysis, Z.V.H., S.Z. and T.Z.; sample fabrication, Z.X., Y.L. and S.Z.; data curation, W.P., Z.X. and X.W.; discussion, W.P., Z.V.H. and S.Z., T.Z.; writing—original draft preparation, W.P.; writing—review and editing, Z.V.H., S.Z. and T.Z. All authors have read and agreed to the published version of the manuscript.

**Funding:** This research was funded by the National Key R&D Program of China (2019YFA0307800), the National Natural Science Foundation of China (NSFC) (Grant Nos. 92265203, 12004259, 12204287, and 11974357), and the China Postdoctoral Science Foundation (Grant No. 2022M723215).

**Institutional Review Board Statement:** Not applicable.

**Informed Consent Statement:** Not applicable.

**Data Availability Statement:** Data is available from the corresponding author on reasonable request.

**Acknowledgments:** The authors appreciate the fruitful discussions with Yunfei Qi.

**Conflicts of Interest:** The authors declare no conflict of interest.

#### References

1. Novoselov, K.S.; Geim, A.K.; Morozov, S.V.; Jiang, D.E.; Zhang, Y.; Dubonos, S.V.; Grigorieva, I.V.; Firsov, A.A. Electric field effect in atomically thin carbon films. *Science* **2004**, *306*, 666–669. [[CrossRef](#)] [[PubMed](#)]
2. Ahn, E.C. 2D materials for spintronic devices. *NPJ 2D Mater. Appl.* **2020**, *4*, 17. [[CrossRef](#)]
3. Novoselov, K.S.; Jiang, D.; Schedin, F.; Booth, T.J.; Khotkevich, V.V.; Morozov, S.V.; Geim, A.K. Two-dimensional atomic crystals. *Proc. Natl. Acad. Sci. USA* **2005**, *102*, 10451–10453. [[CrossRef](#)] [[PubMed](#)]
4. Novoselov, K.S.; Mishchenko, A.; Carvalho, O.A.; Castro Neto, A.H. 2D materials and van der Waals heterostructures. *Science* **2016**, *353*, aac9439. [[CrossRef](#)] [[PubMed](#)]
5. Chuang, P.; Ho, S.C.; Smith, L.W.; Sfigakis, F.; Pepper, M.; Chen, C.H.; Fan, J.C.; Griffiths, J.P.; Farrer, I.; Beere, H.E.; et al. All-electric all-semiconductor spin field-effect transistors. *Nat. Nanotechnol.* **2015**, *10*, 35–39. [[CrossRef](#)]
6. Wang, K.L.; Alzate, J.G.; Amiri, P.K. Low-power non-volatile spintronic memory: STT-RAM and beyond. *J. Phys. D Appl. Phys.* **2013**, *46*, 074003. [[CrossRef](#)]
7. Behin-Aein, B.; Datta, D.; Salahuddin, S.; Datta, S. Proposal for an all-spin logic device with built-in memory. *Nat. Nanotechnol.* **2010**, *5*, 266–270. [[CrossRef](#)]
8. Rahman, S.; Torres, J.F.; Khan, A.R.; Lu, Y. Recent developments in van der Waals antiferromagnetic 2D materials: Synthesis, characterization, and device implementation. *ACS Nano* **2021**, *15*, 17175–17213. [[CrossRef](#)]
9. Huang, B.; Clark, G.; Navarro-Moratalla, E.; Klein, D.R.; Cheng, R.; Seyler, K.L.; Zhong, D.; Schmidgall, E.; McGuire, M.A.; Cobden, D.H.; et al. Layer-dependent ferromagnetism in a van der Waals crystal down to the monolayer limit. *Nature* **2017**, *546*, 270–273. [[CrossRef](#)]
10. Wang, X.; Sun, Y.; Liu, K. Chemical and structural stability of 2D layered materials. *2D Mater.* **2019**, *6*, 042001. [[CrossRef](#)]
11. Wang, X.; Fan, W.; Fan, Z.; Dai, W.; Zhu, K.; Hong, S.; Sun, Y.; Wu, J.; Liu, K. Substrate modified thermal stability of mono- and few-layer  $\text{MoS}_2$ . *Nanoscale* **2018**, *10*, 3540–3546. [[CrossRef](#)]
12. Kostoglou, N.; Polychronopoulou, K.; Rebholz, C. Thermal and chemical stability of hexagonal boron nitride (h-BN) nanoplatelets. *Vacuum* **2015**, *112*, 42–45. [[CrossRef](#)]
13. Fan, X.; Zheng, W.T.; Kuo, J.L.; Singh, D.J. Structural stability of single-layer  $\text{MoS}_2$  under large strain. *J. Phys. Condens. Matter* **2015**, *27*, 105401. [[CrossRef](#)]

14. Yang, S.; Park, S.; Jang, S.; Kim, H.; Kwon, J.Y. Electrical stability of multilayer MoS<sub>2</sub> field-effect transistor under negative bias stress at various temperatures. *Phys. Status Solidi RRL–Rapid Res. Lett.* **2014**, *8*, 714–718. [[CrossRef](#)]
15. Gong, C.; Li, L.; Li, Z.; Ji, H.; Stern, A.; Xia, Y.; Cao, T.; Bao, W.; Wang, C.; Wang, Y.; et al. Discovery of intrinsic ferromagnetism in two-dimensional van der Waals crystals. *Nature* **2017**, *546*, 265–269. [[CrossRef](#)]
16. Shcherbakov, D.; Stepanov, P.; Weber, D.; Wang, Y.; Hu, J.; Zhu, Y.; Watanabe, K.; Taniguchi, T.; Mao, Z.; Windl, W.; et al. Raman spectroscopy, photocatalytic degradation, and stabilization of atomically thin chromium tri-iodide. *Nano Lett.* **2018**, *18*, 4214–4219. [[CrossRef](#)]
17. Osváth, Z.; Darabont, A.; Nemes-Incze, P.; Horváth, E.; Horváth, Z.E.; Biró, L.P. Graphene layers from thermal oxidation of exfoliated graphite plates. *Carbon* **2007**, *45*, 3022–3026. [[CrossRef](#)]
18. Avachev, A.; Vikhrov, S.P.; Vishnyakov, N.V.; Kozyukhin, S.A.; Mitrofanov, K.V.; Terukov, E.I. Phase transitions in thin GeSbTe chalcogenide films according to Raman spectroscopy data. *Semiconductors* **2012**, *46*, 591–594. [[CrossRef](#)]
19. Tu, Z.; Xie, T.; Lee, Y.; Zhou, J.; Admasu, A.S.; Gong, Y.; Valanoor, N.; Cumings, J.; Cheong, S.W.; Takeuchi, I.; et al. Ambient effect on the Curie temperatures and magnetic domains in metallic two-dimensional magnets. *NPJ 2D Mater. Appl.* **2021**, *5*, 62. [[CrossRef](#)]
20. Ji, H.; Stokes, R.A.; Alegria, L.D.; Blomberg, E.C.; Tanatar, M.A.; Reijnders, A.; Schoop, L.M.; Liang, T.; Burch, K.S.; Ong, N.P.; et al. A ferromagnetic insulating substrate for the epitaxial growth of topological insulators. *J. Appl. Phys.* **2013**, *114*, 114907. [[CrossRef](#)]
21. Martin, M.-B.; Dlubak, B.; Weatherup, R.S.; Yang, H.; Deranlot, C.; Bouzehouane, K.; Petroff, F.; Anane, A.; Hofmann, S.; Robertson, J.; et al. Sub-nanometer atomic layer deposition for spintronics in magnetic tunnel junctions based on graphene spin-filtering membranes. *ACS Nano* **2014**, *8*, 7890–7895. [[CrossRef](#)] [[PubMed](#)]
22. Galbiati, M.; Zatzko, V.; Godel, F.; Hirschauer, P.; Vecchiola, A.; Bouzehouane, K.; Collin, S.; Servet, B.; Cantarero, A.; Petroff, F.; et al. Very long term stabilization of a 2d magnet down to the monolayer for device integration. *ACS Appl. Electron. Mater.* **2020**, *2*, 3508–3514. [[CrossRef](#)]
23. Lohmann, M.; Su, T.; Niu, B.; Hou, Y.; Alghamdi, M.; Aldosary, M.; Xing, W.; Zhong, J.; Jia, S.; Han, W.; et al. Probing magnetism in insulating Cr<sub>2</sub>Ge<sub>2</sub>Te<sub>6</sub> by induced anomalous Hall effect in Pt. *Nano Lett.* **2019**, *19*, 2397–2403. [[CrossRef](#)] [[PubMed](#)]
24. Sandilands, L.J.; Shen, J.X.; Chugunov, G.M.; Zhao, S.Y.F.; Ono, S.; Ando, Y.; Burch, K.S. Stability of exfoliated Bi<sub>2</sub>Sr<sub>2</sub>Dy<sub>x</sub>Ca<sub>1-x</sub>-Cu<sub>2</sub>O<sub>8+δ</sub> studied by Raman microscopy. *Phys. Rev. B* **2010**, *82*, 064503. [[CrossRef](#)]
25. Zhao SY, F.; Beekman, C.; Sandilands, L.J.; Bashucky JE, J.; Kwok, D.; Lee, N.; LaForge, A.D.; Cheong, S.W.; Burch, K.S. Fabrication and characterization of topological insulator Bi<sub>2</sub>Se<sub>3</sub> nanocrystals. *Appl. Phys. Lett.* **2011**, *98*, 141911. [[CrossRef](#)]
26. Rudolf, T.; Kant, C.; Mayr, F.; Loidl, A. Magnetic-order induced phonon splitting in MnO from far-infrared spectroscopy. *Phys. Rev. B* **2008**, *77*, 024421. [[CrossRef](#)]
27. Lin, M.-W.; Zhuang, H.L.; Yan, J.; Ward, T.Z.; Puzos, A.A.; Rouleau, C.M.; Gai, Z.; Liang, L.; Meunier, V.; Sumpter, B.G.; et al. Ultrathin nanosheets of CrSiTe<sub>3</sub>: A semiconducting two-dimensional ferromagnetic material. *J. Mater. Chem. C* **2016**, *4*, 315–322. [[CrossRef](#)]
28. Topsakal, M.; Aktürk, E.; Ciraci, S. First-principles study of two-and one-dimensional honeycomb structures of boron nitride. *Phys. Rev. B* **2009**, *79*, 115442. [[CrossRef](#)]
29. Sun, Y.; Xiao, R.C.; Lin, G.T.; Zhang, R.R.; Ling, L.S.; Ma, Z.W.; Luo, X.; Lu, W.J.; Sun, Y.P.; Sheng, Z.G. Effects of hydrostatic pressure on spin-lattice coupling in two-dimensional ferromagnetic Cr<sub>2</sub>Ge<sub>2</sub>Te<sub>6</sub>. *Appl. Phys. Lett.* **2018**, *112*, 072409. [[CrossRef](#)]
30. Carteaux, V.; Brunet, D.; Ouyard, G.; Andre, G. Crystallographic, magnetic and electronic structures of a new layered ferromagnetic compound Cr<sub>2</sub>Ge<sub>2</sub>Te<sub>6</sub>. *J. Phys. Condens. Matter* **1995**, *7*, 69. [[CrossRef](#)]
31. Mogi, M.; Tsukazaki, A.; Kaneko, Y.; Yoshimi, R.; Takahashi, K.S.; Kawasaki, M.; Tokura, Y. Ferromagnetic insulator Cr<sub>2</sub>Ge<sub>2</sub>Te<sub>6</sub> thin films with perpendicular remanence. *Appl. Mater.* **2018**, *6*, 091104. [[CrossRef](#)]
32. Chen, L.; Cao, Z.Y.; Yu, H.; Jiang, B.B.; Su, L.; Shi, X.; Chen, L.; Chen, X.J. Phonon Anharmonicity in Thermoelectric Palladium Sulfide by Raman Spectroscopy. *Appl. Phys. Lett.* **2018**, *113*, 022105. [[CrossRef](#)]
33. Wang, Z.; Zhang, T.; Ding, M.; Dong, B.; Li, Y.; Chen, M.; Li, X.; Huang, J.; Wang, H.; Zhao, X.; et al. Electric-field control of magnetism in a few-layered van der Waals ferromagnetic semiconductor. *Nat. Nanotechnol.* **2018**, *13*, 554–559. [[CrossRef](#)]
34. Zhang, T.; Zhao, S.; Wang, A.; Xiong, Z.; Liu, Y.; Xi, M.; Li, S.; Lei, H.; Han, Z.V.; Wang, F. Electrically and Magnetically Tunable Valley Polarization in Monolayer MoSe<sub>2</sub> Proximitized by a 2D Ferromagnetic Semiconductor. *Adv. Funct. Mater.* **2022**, *32*, 2204779. [[CrossRef](#)]
35. Karpiak, B.; Cummings, A.W.; Zollner, K.; Vila, M.; Khokhriakov, D.; Hoque, A.M.; Dankert, A.; Svedlindh, P.; Fabian, J.; Roche, S.; et al. Magnetic proximity in a van der Waals heterostructure of magnetic insulator and graphene. *2D Mater.* **2019**, *7*, 015026. [[CrossRef](#)]
36. Tian, Y.; Gray, M.J.; Ji, H.; Cava, R.J.; Burch, K.S. Magneto-elastic coupling in a potential ferromagnetic 2D atomic crystal. *2D Mater.* **2016**, *3*, 025035. [[CrossRef](#)]

**Disclaimer/Publisher’s Note:** The statements, opinions and data contained in all publications are solely those of the individual author(s) and contributor(s) and not of MDPI and/or the editor(s). MDPI and/or the editor(s) disclaim responsibility for any injury to people or property resulting from any ideas, methods, instructions or products referred to in the content.